Journal of Applied Electrochemistry **32**: 173–178, 2002.

Composition dependence of the oxygen-evolution reaction rate on $Ir_xTi_{1-x}O_2$ mixed-oxide electrodes

KAZUKI ENDO*, YASUSHI KATAYAMA, TAKASHI MIURA and TOMIYA KISHI
Faculty of Science and Technology, Keio University, Hiyoshi 3-14-1, Kohoku-ku, Yokohama 223-8522, Japan
*(*author for correspondence, e-mail: c08792@educ.cc.keio.ac.jp)*

Received 14 May 2001; accepted in revised form 23 October 2001

Key words: IrO_2, mixed oxide, oxygen evolution, reaction rate, TiO_2

Abstract

Mudcrack-free oxide films of $Ir_xTi_{1-x}O_2$ ($0 < x \leqslant 1$) on titanium substrates were obtained, and the effects of the oxide composition on the rate of oxygen-evolution reaction were investigated. At $x \geqslant 0.6$, Ir-rich grains appear on the mudcrack-free surface. In the purely single-phase region ($0 < x \leqslant 0.5$), the pseudo-capacitive charge is proportional to the surface composition, x_s, and the exchange-current density for the oxygen-evolution reaction increases linearly with x_s at $0.2 \leqslant x_s \leqslant 0.5$, with an extrapolated intercept at $x_s \sim 0.15$, below which the oxides are inactive.

1. Introduction

Precious metal dioxides, such as RuO_2 and IrO_2, which have a high electronic conductivity because of their mixed valence states, are of interest as insoluble anode materials for industrial use [1]. Among these oxides, IrO_2 is known to have excellent wear resistance during oxygen evolution though its electrocatalytic activity is low compared with that of RuO_2 [1]. These properties may be improved by adding a second component, such as valve metal oxides [2]. In the case of the IrO_2–ZrO_2 [3] and IrO_2–Ta_2O_5 [4] binary systems, the two components are immiscible with each other, and the electrocatalytic activity of the binary mixture is controlled by microscopic structural features, such as grain size, morphology, and dispersion state [5]. In the contrasting case of the IrO_2–TiO_2 system, solid solutions of $Ir_xTi_{1-x}O_2$ can be prepared within a range of $0 < x < 0.5$ on a titanium metal substrate [6]. Systematic studies on the electrocatalytic activity of these solid solutions may provide useful information about the role of electronic interactions in binary oxide electrodes. However, the well-known 'cracked mud' morphology and the nonhomogeneous metal distribution of conventional $Ir_xTi_{1-x}O_2$ films obtained by thermal decomposition make it extremely difficult to investigate the x-dependence of the electrocatalytic activity.

In the present work, crack-free $Ir_xTi_{1-x}O_2$ films were successfully prepared, and the rate of oxygen-evolution reaction on these films was investigated in sulfuric acid solution over the whole composition range of $0 < x \leqslant 1$. A similar fundamental study on smooth and cracked RuO_2 film electrodes has already been carried out by Trasatti and coworkers [7].

2. Experimental

2.1. *Preparation of* $Ir_xTi_{1-x}O_2$

$Ir_xTi_{1-x}O_2$ ($0 < x \leqslant 1$) films were prepared on a titanium plate by repeating solution brushing–thermal decomposition cycles, where x denotes the nominal composition based on the mixing ratio of Ir- and Ti-sources. A titanium substrate (Nilaco, 99.5%, $10 \times 10 \times 1$ mm^3) was washed with neutral detergent water in an ultrasonic bath, etched by a 10% oxalic acid solution at 80 °C for 5–180 min, and then rinsed with water and acetone in an ultrasonic bath. Homogeneous coating solutions were prepared by dissolving appropriate amounts of $IrCl_3 \cdot nH_2O$ (Soekawa, Ir 53%) and $C_4H_9O[Ti(OC_4H_9)_2O]_4C_4H_9$ (Wako, 95%) into 1-butanol and stirring for 4–5 days while the total concentration of Ir and Ti was kept constant at 0.26 M [8]. The solution was loaded on the pretreated titanium plates by brushing smoothly, dried at 60 °C for 10 min, and then heated at 450 °C for 10 min. These loading, drying, and decomposing cycles were repeated 6–18 times to obtain 1 μm-thick $Ir_xTi_{1-x}O_2$ based on weight gain.

The coated oxide surface was analyzed by X-ray diffraction (XRD), scanning electron microscopy (SEM), energy dispersive X-ray spectrometry (EDX), and X-ray photoelectron spectroscopy (XPS).

2.2. *Electrochemical measurements*

All electrochemical measurements were carried out in an N_2- or O_2-saturated 0.5 M H_2SO_4 solution at 25 °C. The sample electrodes were covered with silicone rubber to expose only the $Ir_xTi_{1-x}O_2$ surface to the electrolyte after connecting with a copper lead wire on the rear face. A spiral platinum wire was placed in a counter electrode compartment separated from the main electrolyte by a glass filter. An Ag/AgCl electrode in a saturated KCl solution was used as the reference *via* a salt bridge. All the electrode potentials are referred to the reversible hydrogen electrode (RHE).

Cyclic voltammetric measurements were carried out at a sweep rate of 2–100 mV s^{-1} between 0.1 and 1.5 V. Similar measurements were carried out within a narrow (±50 mV) potential range around the redox peak potential. In addition, a steady-state oxygen-evolution current was measured under potentiostatic conditions to obtain Tafel plots, where the set potentials were raised by 10 mV steps from the rest potential.

3. Results and discussions

3.1. *Characterization of oxide films*

Smooth $Ir_xTi_{1-x}O_2$ films without mudcracks, as shown in Figure 1, were obtained by the minimized loading of a mixed starting solution in each loading–drying–decomposing cycle on the Ti substrates, which were etched under mild conditions (10% oxalic acid for 5 min) compared with that typically employed for the preparation of these electrodes (10% oxalic acid for 60 min). About 18 preparation cycles were necessary to obtain a film thickness of 1 μm. At the composition range of $x \geqslant 0.6$, however, the surface became nonhomogeneous, and small particles of 200–300 nm were dispersed on the mudcrack-free surface, as shown in Figure 2. These

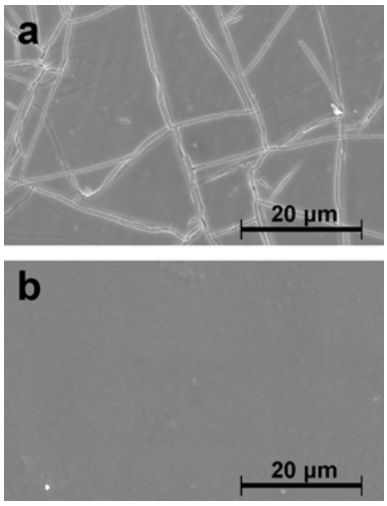

Fig. 1. SEM images of $Ir_{0.3}Ti_{0.7}O_2$. 1-μm oxide loading by (a) 6 cycles; (b) 18 cycles.

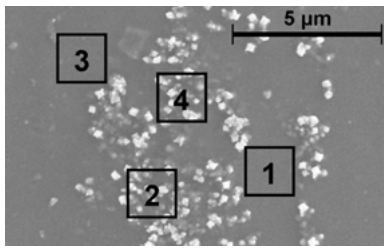

Fig. 2. SEM image of $Ir_{0.6}Ti_{0.4}O_2$ (EDX analysis region 1–4).

Table 1 Atomic percentages of Ir and Ti by EDX.

Region	Ir(%)	Ti(%)
1	58.2	41.8
2	65.8	34.2
3	51.8	48.2
4	62.9	37.1

particles had a higher Ir content than the bulk (see Table 1), though their total amount seemed to be small in a whole film.

A typical XRD pattern of the prepared film is shown in Figure 3. In the entire composition range of $0 < x \leqslant 1$, all the XRD peaks were nearly symmetrical without shoulders and could be attributed to a rutile lattice. Thus, prepared $Ir_xTi_{1-x}O_2$ films were single-phase rutile on an XRD basis. The above-mentioned Ir-rich particles were suspected to be too small in quantity

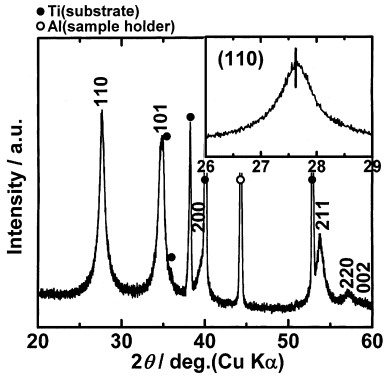

Fig. 3. XRD pattern of $Ir_{0.7}Ti_{0.3}O_2$.

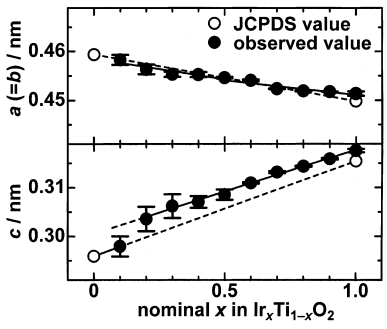

Fig. 4. Dependence of lattice constants on the composition of $Ir_xTi_{1-x}O_2$.

to give any XRD peak. For the purpose of this study, we will assume that all the $Ir_xTi_{1-x}O_2$ films have a homogeneous rutile phase. Figure 4 shows the calculated lattice constants of our samples (solid circles) in comparison to the JCPDS data (open circles) for TiO_2 and IrO_2. Both a ($=b$) and c change almost linearly with the nominal composition x. Although the lattice constant c increases linearly with x at $0.2 \leqslant x < 1.0$, those for TiO_2 and IrO_2 lie below this line. Such disagreement may be caused by the partial replacement of Ir^{IV} by Ir^{III} and H^+, as described below. No change was observed for XRD peak angles, intensities, or widths after additional annealing at 450 °C for 3 h and this fact suggests that the bulk of prepared films has a rutile lattice at this low temperature at least in a metastable phase. The available phase diagram in the Ir–Ti–O system [9] indicates that binary solid solutions exist on both the TiO_2 side (up to a few mol% of IrO_2) and on the IrO_2 side (up to ~10 mol% of TiO_2) at 1000 °C. Roginskaya and Morozova [6], on the other hand, reported single- and two-phase regions at $0.1 \leqslant x < 0.5$ and $0.5 < x < 1.0$, respectively. These facts may suggest that the appearance of such a metastable phase depends on preparation conditions that determine the kinetics of precursor formation, thermal decomposition, and crystallization processes. The size of the rutile grains calculated by using Scherrer's equation increased from ~10 nm at $x = 0.2$ to ~20 nm at x=0.5 and then remained constant at ~20 nm at $0.6 \leqslant x < 1.0$ independently of the crystal orientation. Thus, different decomposition–crystallization mechanisms are also suspected by the observed grain sizes between nominal composition ranges of $x \leqslant 0.5$ and $x \geqslant 0.6$.

Typical Ir4f and O1s spectra could be confirmed by XPS analysis of the films, as shown in Figure 5. The coexistence of Ir^{IV} and Ir^{III} at the surface was supported by split Ir4f peaks. Similarly, split O1s peaks suggested

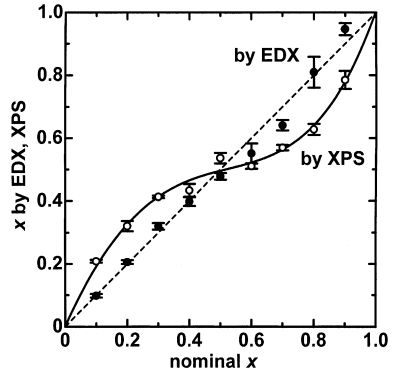

Fig. 6. Surface and bulk composition of $Ir_xTi_{1-x}O_2$ measured by XPS and EDX.

the existence of M—OH groups in addition to M—O. There was an approximate proportionality between Ir^{III} and M—OH intensities. Thus, Ir^{III} is probably accompanied by H^+, such as hydroxide at the oxide surface. The (Ir/Ti) molar ratios near the surface, x_s, determined by $Ir4f_{7/2}$ and $Ti2p_{3/2}$ XPS peak intensities, are plotted against the nominal composition in Figure 6, where rather macroscopic (Ir/Ti) ratios, x_b, indicated by observed EDX data, are superimposed. The bulk composition, x_b, coincides with the nominal composition, whereas Ir- and Ti-enrichment at the surface occur at $x \leqslant 0.5$ and $x \geqslant 0.6$, respectively. The reasons for surface enrichment are suspected to be as follows: the pyrolysis process begins from the hydrolysis of loading a mixed solution and is followed by the formation of polyanion, hydroxide, and oxide. The rate of each process may depend on the (Ir/Ti) ratio. In a Ti-rich case ($x < 0.5$), the pyrolysis process will be dominated by a Ti component, and Ir is incorporated in Ti precursors to produce Ti-covered Ir units. Such a majority-covered minority may lead to the observed surface enrichment of

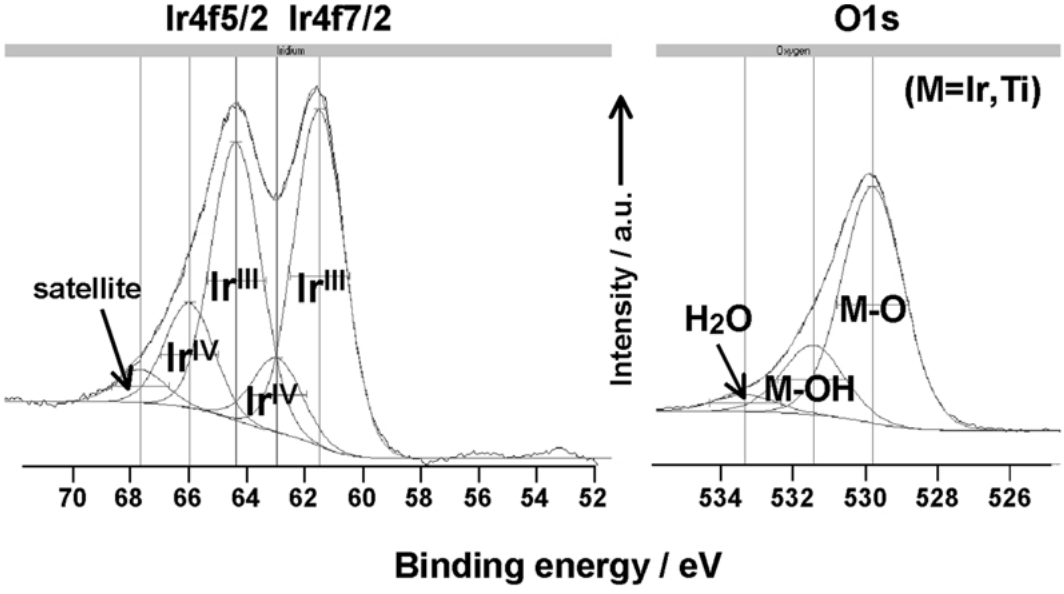

Fig. 5. XPS spectra of $Ir_{0.3}Ti_{0.7}O_2$ (Ir4f and O1s).

the majority component. At the same time, the appearance of Ir-rich small particles at $x \geqslant 0.6$ can also be related to an incorporation rate of an Ir precursor that is too low to give minority-free units. Roginskaya and Morozova [6] proposed a similar model to explain the segregation phenomena in a cracked-mud surface. Battisti and coworkers [10], on the other hand, confirmed the surface enrichment of a Ti component by RBS analysis and explained that it was due to the fact that Ti had stronger affinity for atmospheric oxygen than Ir. Nevertheless, the difference in Ir—O and Ti—O bond strengths does not seem to play as important a role in surface Ir- or Ti-enrichment as the first preparation step of pyrolysis does.

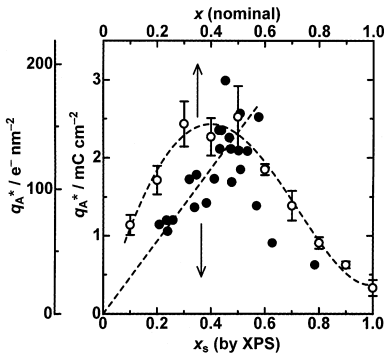

Fig. 8. Dependence of q_A^* on nominal (x) and surface (x_s) compositions.

3.2. *Surface redox behaviors*

Typical cyclic voltammograms of $Ir_xTi_{1-x}O_2$ electrodes scanned between 0.1 and 1.5 V are shown in Figure 7. A cathodic current arising at 1.4 V corresponds to oxygen evolution. A cathodic and an anodic current peak at 0.9 V are attributed to the redox reaction of the Ir^{III}/Ir^{IV} couple in the oxide film. Though these redox peaks are broad, their peak potentials can be regarded as substantially independent of x at $0 < x \leqslant 0.5$. This fact may suggest that the electronic states of Ir do not change remarkably after forming mixed oxides with Ti at $0 < x \leqslant 0.5$. At the composition range of $0.6 \leqslant x \leqslant 1.0$, however, the peak current densities for the Ir^{III}/Ir^{IV} couple decrease with increasing Ir content x, and another redox couple appears with an addition of about 1.3 V. The peak current densities of the new 1.3 V couple tend to decrease similarly with x. According to reports on pure IrO_2 electrodes [11, 12], the redox couple at 1.3 V can be ascribed to either the Ir^{IV}/Ir^{V} or Ir^{IV}/Ir^{VI} reaction. Since IrO_2-rich small grains are present only at $x \geqslant 0.6$, the 1.3 V redox reactions are considered to take place on these grains in addition to the Ir^{III}/Ir^{IV} reactions on the rest of the bulk surface at 0.9 V.

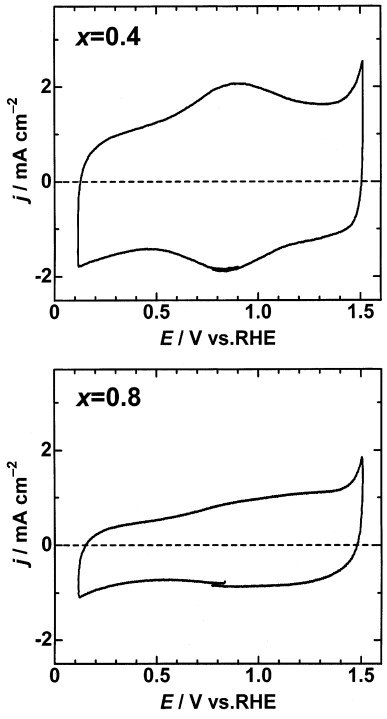

Fig. 7. Cyclic voltammograms of $Ir_{0.4}Ti_{0.6}O_2$ and $Ir_{0.8}Ti_{0.2}O_2$ electrodes in 0.5 M H_2SO_4; scan rate 100 mV s^{-1}.

Both anodic and cathodic peak-current densities of the 0.9 V couple are proportional to the scan rates (v) from 10 to 100 mV s^{-1}, and, therefore, its voltammetric charge remains constant. However, the same voltammetric charge tends to increase with v in a lower range (<10 mV s^{-1}), probably because the charging of the inner sites is involved, as proposed by Trasatti and coworkers [13]. Therefore, we define here the pseudocapacitive charge, q^*, by the v-independent voltammetric charge, which is consumed to charge the outermost sites on the electrode surface. Strictly, a small fraction of a pure double-layer charge [1] may be involved in the thus-determined q^* in addition to Ir^{III}/Ir^{IV} redox processes. Such a q^* value is independent of v after expanding the sweep limits from ±50 mV of the Ir^{III}/Ir^{IV} middle-peak potential to a wider range of 0.1–1.5 V. The given q^* values in this paper are from the former narrow scanning.

The q^* values can be regarded to be proportional to the surface density of an active Ir site, as described in a report by Burke and Whelan [11]. The anodic side charge q_A^* was comparatively plotted in Figure 8 against the nominal and surface compositions described above. While q_A^* increases with x at $x \leqslant 0.5$, it begins to decrease at $x \geqslant 0.6$. Similar results of the q_A^* maxima at $x = 0.6$ by Trasatti and coworkers [14] or at $x = 0.3$ by Kristóf and coworkers [15] have already been reported for $Ir_xTi_{1-x}O_2$ electrodes. Decreased porosity due to crystallite growth [14] or morphology changes by segregation [15] may explain the decrease in q_A^* after passing the maximum. Crystallite growth is possibly responsible for the decrease in q_A^* at $x \geqslant 0.6$ in our case because it is confirmed by the width of XRD peaks. On the other hand, q_A^* increases almost linearly with the surface composition at $x_s \leqslant 0.5$, indicating that the

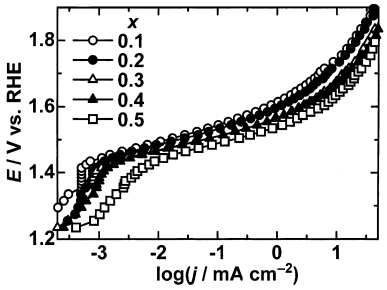

Fig. 9. Potentiostatic steady-state current–potential curves for O_2-evolution reaction on $Ir_xTi_{1-x}O_2$ ($0.1 \leqslant x \leqslant 0.5$) electrodes in 0.5 M H_2SO_4.

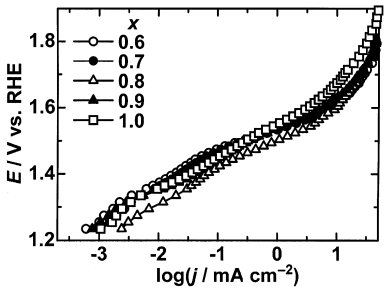

Fig. 10. Potentiostatic steady-state current–potential curves for O_2-evolution reaction on $Ir_xTi_{1-x}O_2$ ($0.6 \leqslant x \leqslant 1.0$) electrodes in 0.5 M H_2SO_4.

density of active Ir sites on the outer surface is proportional to x_s.

3.3. *Oxygen evolution on $Ir_xTi_{1-x}O_2$ electrodes*

Typical current–potential curves for oxygen-evolution on $Ir_xTi_{1-x}O_2$ electrodes in 0.5 M H_2SO_4 are shown in Figure 9 ($0.1 \leqslant x \leqslant 0.5$) and Figure 10 ($0.6 \leqslant x \leqslant 1.0$). For $x \leqslant 0.5$, Tafel lines having an x-independent slope of 60 mV decade^{-1} are confirmed at $E > 1.45$ V. For $x \leqslant 0.6$, on the other hand, there are two Tafel lines having a slope of ~90 mV decade^{-1} at $E < 1.45$ V or of 60–90 mV decade^{-1} at $E > 1.45$ V. In the former Tafel region, some parallel reaction, such as surface oxidation, might be involved.

The slopes of the latter Tafel line increase with x, as can be seen in Figure 11, and they are large compared with the reported slope (40–60 mV decade^{-1}) for mud-cracked electrodes by Trasatti and coworkers [14]. The effects of mudcracks on the chlorine-evolution electrocatalysis have already been discussed for RuO_2 electrodes [7], and the existing mudcracks might affect the surface coverage of intermediates or lead to different rate-determining steps in general. Based on the oxygen-evolution reaction mechanism proposed by Bockris and coworkers [16], Bockris and Otagawa [17], Trasatti and coworkers [14, 18] proposed the following steps:

$$S + H_2O \rightarrow S{-}OH^* + H^+ + e^- \quad (1)$$

$$S{-}OH^* \rightarrow S{-}OH \quad (2)$$

$$S{-}OH \rightarrow S{-}O + H^+ + e^- \quad (3)$$

$$S{-}O + S{-}O \rightarrow O_2 + 2\,S \quad (4)$$

A Tafel slope of 40 mV decade^{-1} is expected for the rate-determining step of (3) as applied for the mudcrack surface [14]. If the surface coverage of S—OH is large enough, then reaction (2) becomes rate-determining to give the Tafel slope of 60 mV decade^{-1}, as observed in this study at $x \leqslant 0.5$. Because we have to take into account the complexity of surface inhomogeneity at a nominal composition range of $x \geqslant 0.6$, further discussions will be focused on the homogeneous surface at $x \leqslant 0.5$.

Exchange-current densities (j_0) determined by extrapolating Tafel lines to the reversible oxygen-evolution potential (Figure 9) were plotted in Figure 12 against the surface composition. The exchange-current density, after being divided by a pseudo-capacitive charge, j_0/q_A^*, should give a measure for the electrocatalytic activity per unit active site, which is also superimposed in Figure 12. The exchange-current density increases almost linearly with increasing x_s from 0.5 to 5 nA cm^{-2}, where the extrapolation of this line gives completely diminished activity at $x_s \sim 0.15$. This result probably indicates that Ir on the surface does not act as an oxygen-evolution site until its population exceeds $x_s = 0.15$.

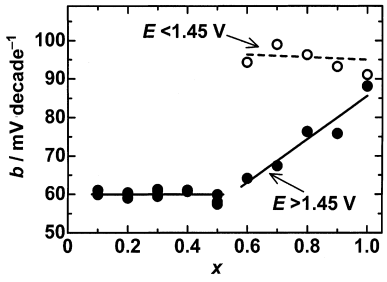

Fig. 11. Tafel slopes for O_2-evolution reaction on $Ir_xTi_{1-x}O_2$ electrodes in 0.5 M H_2SO_4.

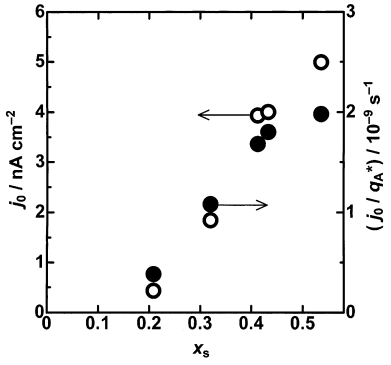

Fig. 12. Dependence of exchange-current density j_0 and j_0/q_A^* for O_2-evolution reaction on surface composition, x_s.

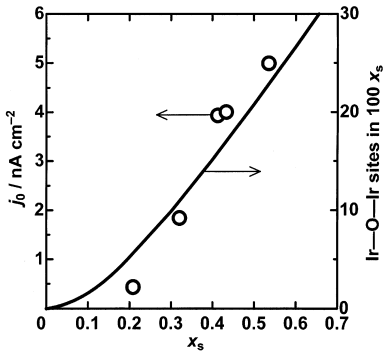

Fig. 13. Dependence of j_0 for O_2-evolution reaction and coupled-iridium sites on surface composition, x_s.

The concept of the minimum surface population of Ir may be elucidated as follows: in a series of reactions (1)–(4), water molecules adsorbed on active site S are oxidized to S—O, and oxygen evolves finally through step (4), the so-called atom–atom step [19, 20]. Therefore, two sites must be adjacent in order to let two oxygen atoms combine in step (4). Assuming the rate-determining step of (2) and the absolute inactivity of Ti, the population of adjacent Ir–Ir pairs should determine the electrocatalytic activity. The statistical model calculation was carried out for the probability that two Ir atoms are nearest to each other on the surface lattice. Such a calculation was repeated 1000 times for each Ir/Ti ratio based on the randomized distribution of Ir and Ti on the 10×10 grids, and the average number of adjacent Ir–Ir couples was determined as shown in Figure 13. As seen in this figure, the number of adjacent Ir–Ir couples is not proportional to the surface concentration of Ir, x_s, but increases sharply with x_s, as if observed for the j_0–x_s relationship. This fact suggests that adjacent Ir–Ir couples play important roles in electrocatalysis, though further detail and a quantitative model should be considered.

Finally, an exceptional case of $x = 0.1$ will be discussed. The lattice constant c of the same oxide lies on a straight line between two JCPDS items for pure TiO_2 and pure IrO_2 in contrast to other oxide films of $0.2 \leqslant x \leqslant 1.0$, as shown in Figure 4. This fact suggests that a thermodynamically stable solid solution was prepared only at x=0.1 and that the rest of the mixed oxides at $0.2 \leqslant x \leqslant 1.0$ were probably metastable solid solutions with higher electroactivity than the stable ones.

4. Conclusions

A series of $Ir_xTi_{1-x}O_2$ $(0 < x \leqslant 1)$ films without mud-cracks could be obtained by optimizing the preparation conditions on a titanium substrate. Compared with the nominal composition, Ir was enriched and depleted on the film surface at $x \leqslant 0.5$ and $x \geqslant 0.6$, respectively. At the same time, the pseudo-capacitive nature of these oxide electrodes changed drastically at $x = 0.5$, suggesting that redox reactions of Ir might be different at $x \leqslant 0.5$ and $x \leqslant 0.6$, where Ir-enriched small particles coexisted on a smooth surface. As for strictly single-phase oxides at $x \leqslant 0.5$, a pseudo-capacitive charge was proportional to the (Ir/Ti) ratio at the surface, x_s, and the exchange-current density for oxygen-evolution reaction increased nearly linearly with x_s at $0.2 \leqslant x_s \leqslant 0.5$. When x_s became smaller than $\sim$0.15, such an electrode was considered to lose the electrocatalytic activity for oxygen evolution, probably because adjacent Ir–Ir pairs on the surface were required to let two oxygen atoms combine with each other.

References

1. S. Trasatti and G. Lodi, In *Electrodes of Conductive Metallic Oxides Parts A*, S. Trasatti (Ed.) Elsevier, Amsterdam, 1980 p. 301.
2. S. Trasatti, *Electrochim. Acta* **36** (1991) 225.
3. A. Benedetti, P. Riello, G. Battaglin, A. De Battisti and A. Barbieri, *J. Electroanal. Chem.* **376** (1994) 195.
4. R. Otogawa, M. Morimitsu and M. Matsunaga, *Electrochim. Acta* **44** (1998) 1509.
5. C. Comninellis and G.P. Vercesi, *J. Appl. Electrochem.* **21** (1991) 335.
6. Y.E. Roginskaya and O.V. Morozova, *Electrochim. Acta* **40** (1995) 817.
7. S. Ardizzone, A. Carugati, G. Lodi and S. Trasatti, *J. Electrochem. Soc.* **129** (1982) 1689.
8. K. Tsukada, K. Kameyama, K. Yahikozawa and Y. Takasu, *Denki Kagaku* (*currently Electrochemistry*), **61** (1993) 435 (in Japanese).
9. M.K. Reser (Ed.), *Phase Diagrams for Ceramists* (American Ceramic Society, Columbus, 1969), Figure 2180.
10. A. de Battisti, A. Barbieri, A. Giatti, G. Battaglin, S. Daolio and A.B. Boscoletto, *J. Mater. Chem.* **1** (1991) 191.
11. L.D. Burke and D.P. Whelan, *J. Electroanal. Chem.* **124** (1981) 333.
12. A. de O-Sousa, M.A.S. da Silva, S.A.S. Machado, L.A. Avaca and P. de L-Neto, *Electrochim. Acta* **45** (2000) 4467.
13. S. Ardizzone, G. Fregonara and S. Trasatti *Electrochim. Acta* **35** (1990) 263.
14. L.A. da Silva, V.A. Alves, M.A.P. da Silva, S. Trasatti and J.F.C. Boodts, *Can. J. Chem.* **75** (1997) 1483.
15. J. Kristóf, J. Liszi, P. Szabó, A. Barbieri and A. de Battisti, *J. Appl. Electrochem.* **23** (1993) 615.
16. A. Damjanovic, A. Dey and J.O'M. Bockris, *Electrochim. Acta* **11** (1966) 791.
17. J.O'M. Bockris and T. Otagawa, *J. Phys. Chem.* **87** (1983) 2960.
18. L.A. da Silva, V.A. Alves, S. Trasatti and J.F.C. Boodts, *J. Electroanal. Chem.* **427** (1997) 97.
19. N. Furuya and S. Motoo, *J. Electroanal. Chem.* **72** (1976) 165.
20. S. Motoo, *Denki Kagaku* (*currently Electrochemistry*), **48** (1980) 328 (in Japanese).